Published OnlineFirst March 2, 2021; DOI: 10.1158/2159-8290.CD-20-0987

RESEARCH ARTICLE

CD4 T Cell–Dependent Rejection of Beta-2 Microglobulin Null Mismatch Repair–Deficient Tumors

Giovanni Germano[1,2], Steve Lu[3], Giuseppe Rospo[1,2], Simona Lamba[1], Benoit Rousseau[4], Sonia Fanelli[1,2], Denise Stenech[1,2], Dung T. Le[5], John Hays[6], Maria Grazia Totaro[7], Vito Amodio[1,2], Rosaria Chilà[2,7], Anna Mondino[8], Luis A. Diaz Jr.[4], Federica Di Nicolantonio[1,2], and Alberto Bardelli[1,2]

ABSTRACT Inactivation of beta-2 microglobulin (B2M) is considered a determinant of resistance to immune checkpoint inhibitors (ICPi) in melanoma and lung cancers. In contrast, *B2M* loss does not appear to affect response to ICPis in mismatch repair–deficient (MMRd) colorectal tumors where biallelic inactivation of *B2M* is frequently observed. We inactivated *B2m* in multiple murine MMRd cancer models. Although MMRd cells would not readily grow in immunocompetent mice, MMRd *B2m* null cells were tumorigenic and regressed when treated with anti–PD-1 and anti-CTLA4. The efficacy of ICPis against MMRd *B2m* null tumors did not require $CD8^+$ T cells but relied on the presence of $CD4^+$ T cells. Human tumors expressing low levels of B2M display increased intratumoral $CD4^+$ T cells. We conclude that B2M inactivation does not blunt the efficacy of ICPi in MMRd tumors, and we identify a unique role for $CD4^+$ T cells in tumor rejection.

SIGNIFICANCE: *B2M* alterations, which impair antigen presentation, occur frequently in microsatellite-unstable colorectal cancers. Although in melanoma and lung cancers *B2M* loss is a mechanism of resistance to immune checkpoint blockade, we show that MMRd tumors respond to ICPis through $CD4^+$ T-cell activation.

[1]Candiolo Cancer Institute, FPO-IRCCS, Candiolo, Turin, Italy. [2]Department of Oncology, University of Torino, Candiolo, Turin, Italy. [3]Ludwig Center and Howard Hughes Medical Institute at Johns Hopkins, Baltimore, Maryland. [4]Division of Solid Tumor Oncology, Department of Medicine, Memorial Sloan Kettering Cancer Center, New York, New York. [5]Department of Oncology, Sidney Kimmel Comprehensive Cancer Center at Johns Hopkins, Baltimore, Maryland. [6]Division of Medical Oncology, Wexner Medical Center and James Cancer Hospital, The Ohio State University, Columbus, Ohio. [7]IFOM–the FIRC Institute of Molecular Oncology, Milan, Italy. [8]Division of Immunology, Transplantation and Infectious Diseases, IRCCS San Raffaele Scientific Institute, Milan, Italy.

Note: Supplementary data for this article are available at Cancer Discovery Online (http://cancerdiscovery.aacrjournals.org/).

Corresponding Authors: Alberto Bardelli, Candiolo Cancer Institute, FPO-IRCCS, Strada Provinciale 142, km 3.95, Candiolo 10060, Torino, Italy. Phone: 39-011-9933235; E-mail: alberto.bardelli@unito.it; and Giovanni Germano, Phone: 39-011-9933223; E-mail: giovanni.germano@unito.it

Cancer Discov 2021;11:1844–59

doi: 10.1158/2159-8290.CD-20-0987

Published OnlineFirst March 2, 2021; DOI: 10.1158/2159-8290.CD-20-0987

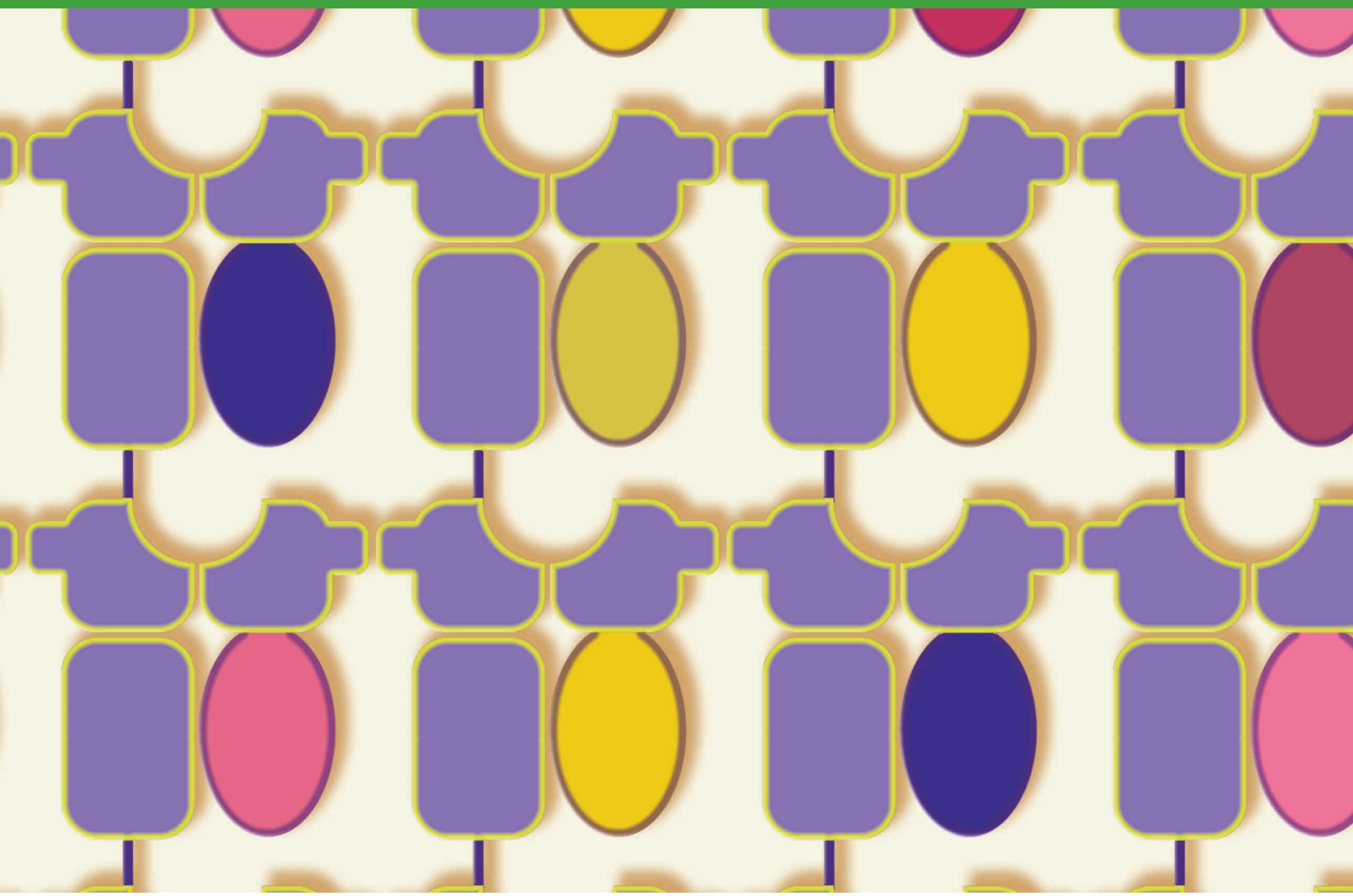

INTRODUCTION

Immune therapies based on anti-CTLA4 and anti-PD-1/PD-L1 checkpoint inhibitors can induce long-lasting responses and improve the overall survival of patients affected by distinct tumor types, including non–small cell lung cancer, melanoma, head and neck cancer, and renal cell carcinoma (1–4). Immune checkpoint inhibitors (ICPi) are also approved to treat patients carrying mismatch repair–deficient (MMRd) tumors (5–7). Inactivation of DNA MMR leads to microsatellite instability (MSI) and generates hypermutated cancers with increased numbers of neoantigens. A large proportion of MSI tumors display long-lasting responses when challenged with immune modulators (7–10).

Tumors may evade immune control mainly due to alterations in the antigen-presenting mechanism (APM; ref. 11). Several studies have reported that molecular defects in the APM represent a possible mechanism of acquired resistance to ICPis in melanoma and lung tumors (12–14). The APM is pivotal for proper processing and presentation of neoantigens by the human leukocyte antigen (HLA) complex at the surface of cancer cells (15). The APM elicits its function as part of a complex mechanism that includes several steps. Upon poly-ubiquitination of proteins, proteasome-mediated protein degradation leads to peptide formation (16). The heavy chain of classic major histocompatibility (MHC) class I molecules is folded and dimerizes with beta-2 microglobulin (B2M) in the endoplasmic reticulum. Calnexin prevents the aggregation of heavy chain which is then receptive for B2M. Next, calreticulin assists in associating the heavy-chain B2M to the peptide loading and assembly complex, which consists of the protein disulfide isomerase ERp57, TAPBP, and the TAP1/2 proteins, and it is key for loading peptides onto the MHC class I binding groove (17). Subsequently, the assembly complex dissociates from the MHC class I B2M, allowing passage from the endoplasmic reticulum to the Golgi and then to the plasma membrane (18). B2M is essential for proper functioning of the MHC class I heavy chain by altering its conformation and enhancing the ability to bind peptides (19). With few exceptions (18, 20), in the absence of B2M, free MHC class I heavy chain is retained in the endoplasmic reticulum, translocated in the cytosol, and eventually degraded (21). Alterations in genes implicated in APM are prevalent in MMRd colorectal cancers (14, 22). In MSI colorectal tumors, *B2M* loss is the second most frequent biallelic disruption after *APC* (11). In a study involving

Published OnlineFirst March 2, 2021; DOI: 10.1158/2159-8290.CD-20-0987

two patient cohorts, loss of MHC class I surface expression was reported to occur in 73% to 78% of MMRd colorectal cancers (23). In an independent cohort, it was found that 24% of MSI colorectal cancers harbored *B2M* mutations, which led to complete loss of B2M protein expression in 73% of the cases (24). A third study found *B2M* mutations in 19 out of 56 MSI colorectal cancers (25).

Biallelic loss of *B2M* impairs HLA-dependent antigen presentation, a phenotype linked to cancer immune tolerance (26). Although alterations in APM are detrimental and commonly lead to resistance to single-agent anti–PD-1 or anti-CTLA4 in carcinoma of the lung and melanoma (12, 13), it has surprisingly been reported that 11 out of 13 patients with MMRd colorectal cancer (85%) with altered *B2M* achieved clinical benefit upon treatment with anti–PD-1 or anti-PD-L1 therapies (5, 6, 24). The molecular and functional bases underlying the diverse impact of *B2M* inactivation among distinct tumor types remain to be explored. It is also unknown whether B2M deficiency could modulate responses to ICPis in MMRd tumors of non-colorectal origin. Understanding the mechanisms modulating immunotherapy outcome in MMRd tumors lacking B2M may help to decipher the role of HLA class I in the response to ICPis and inform precision oncology strategies for tumors with *B2M* loss. To address these aspects, we functionally evaluated the impact of *B2M* loss in immune evasion and resistance to ICPis in colorectal, pancreatic, and breast cancer murine cell lines with or without functional MMR.

RESULTS

Genetic Inactivation of *B2m* Abrogates MHC Class I–Restricted Neoantigen Presentation in MMRd Tumors

In colorectal cancer and other tumor types, MSI results from either mutations or epigenetic silencing of *MLH1*, which is involved in repairing DNA mismatches (27). We previously genetically deleted *Mlh1* in colorectal (CT26) and breast (TS/A) murine cancer lines and in a genetically engineered mouse model (GEMM)–derived pancreatic ductal adenocarcinoma cancer (PDAC) cell line (8). The derivative cells are MMRd and have increased mutational burden; furthermore, *Mlh1* knockout (KO) cells display dynamic mutational profiles that vary over time and do not readily grow in syngeneic immunocompetent mice (8).

To generate MMRd tumors lacking a functional APM, we used CRISPR/Cas9-mediated genetic editing to disable the *B2m* gene in CT26 cells in which *Mlh1* had been previously inactivated. *B2m* KO cells did not express the B2M protein (Fig. 1A). Because it has been reported that Cas9 (a bacterial protein) can affect immune response, we verified that the genetically engineered *Mlh1* KO cells did not express Cas9 (Fig. 1A). CT26 with *B2m* loss had no MHC class I expression on the cell surface (Fig. 1B), an event that is known to blunt MHC class I–dependent neoantigen presentation in the immune compartment (26). In cancer cells, MHC class I protein levels are known to be modulated by IFNγ (28). We found that IFNγ stimulated cell surface expression of MHC class I in *B2m* wild-type cells, but not in their *B2m* KO counterparts (Supplementary Fig. S1). This indicates that, although IFNγ responsiveness is operational in MMRd cell lines, it cannot rescue MHC class I in cells lacking B2M.

Two independent *Mlh1* KO clones were expanded, and their single nucleotide variants (SNV) and insertion/deletion (indel) profiles were assessed. We confirmed the absence of MLH1 and Cas9 proteins (Fig. 1C) and that *Mlh1* KO cells had developed MSI (Fig. 1D; Supplementary Fig. S2). Additionally, based on the number of predicted neoantigens in *Mlh1* KO cells, MMR alterations resulted in an increased number of potential non–self-peptides (Fig. 1E).

B2m Inactivation Restores the Tumorigenic Potential of MMRd in Immunocompetent Mice

We have previously shown that, as compared with their parental counterparts, MMRd cells have impaired tumorigenicity in immune-competent but not in immune-deficient mice (8). We used the same approach to establish how genetic *B2m* inactivation influences immune surveillance against MMRd cancer cells and thus affects tumor growth. To this end, we injected MMRd isogenic cancer cells with or without *B2m* in immune-proficient mice (Fig. 2A). We found that the loss of *B2m* fully restored the tumorigenic potential of MMRd colorectal cancer cells, leading to the rapid development of sizeable tumors in all mice. Overall, these results indicate that the loss of *B2m* enables MMRd tumors to escape immune surveillance.

Although it has been shown that patients bearing MSI colorectal cancer with alterations in *B2M* can respond to ICPis (24), little is known about whether and to what extent *B2M* inactivation affects immunotherapy efficacy in MMRd tumors other than colorectal cancer. To address this, we focused on pancreatic and breast tumors, as they are known to be largely unresponsive to ICPis, unless they carry alterations in MMR (29, 30). We genetically deleted *Mlh1* in breast cancer cells (TS/A) and PDAC cells (Supplementary Fig. S3A), which were subsequently expanded up to the acquisition of MSI (Supplementary Fig. S3B). As observed in colorectal cancer cells, in these tumor types *Mlh1* inactivation also increased the mutational and neoantigen burden (Supplementary Fig. S3C), and *B2m* inactivation (Supplementary Fig. S4A and S4B) abrogated MHC class I cell surface expression (Supplementary Fig. S4C and S4D). Next, we injected isogenic MMR-proficient and MMR-deficient cancer cells with or without *B2m* in immune-competent mice. In agreement with the results observed in colorectal cancer, loss of *B2m* fully restored the tumorigenic potential of MMRd PDAC cells (Supplementary Fig. S5A and S5B) and TS/A cells (Supplementary Fig. S5C and S5D).

Efficacy of ICPis in Mouse Models with MMRd Tumors Lacking *B2m*

We next investigated how the absence of class I–dependent antigen presentation (due to *B2m* loss) affects responses of MMRd cancers to ICPis. To this end, we injected isogenic MMR-proficient and MMR-deficient CT26 cells, either expressing B2M or not, in immune-competent mice and administered anti–PD-1 monoclonal antibody (mAb) when tumors reached a volume of 60 mm^3 (Fig. 2B). Although PD-1 blockade delayed the growth of *B2m* KO MMRd cells, it failed to promote a protective response against *B2m* KO MMR-proficient cells (Fig. 2B).

Published OnlineFirst March 2, 2021; DOI: 10.1158/2159-8290.CD-20-0987

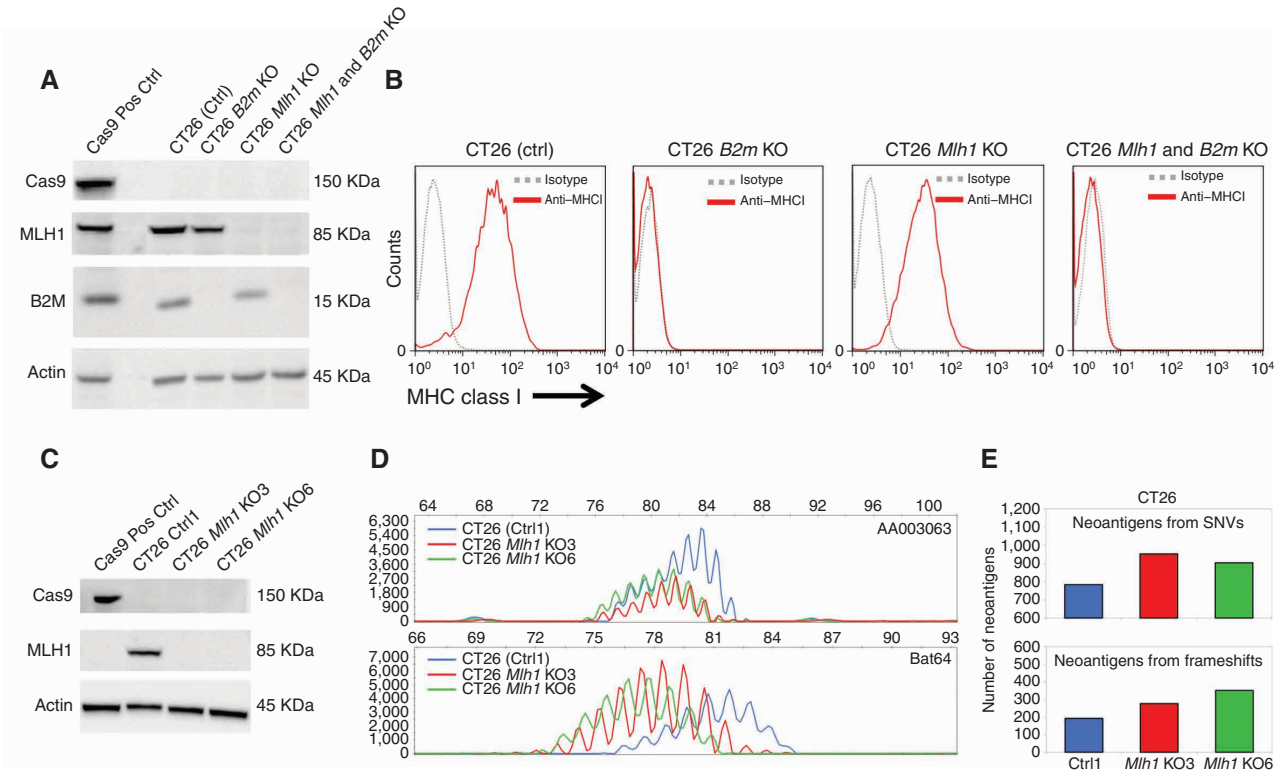

Figure 1. *B2m* inactivation impairs antigen presentation and restores the tumorigenic ability of MMRd colorectal cancer cells. **A,** Western blot analysis of MLH1, B2M, and Cas9 in CT26 clones. **B,** Surface expression of MHC class I in CT26 ctrl, *Mlh1* KO, *B2m* KO. and *Mlh1/B2m* KO measured by FACS. The dotted lines correspond to staining with isotype control antibody. *B2m* genetic inactivation leads to the loss of surface MHC class I expression. **C,** CT26 cells were transiently transfected with a CRISPR/Cas9 construct, and Cas9/MLH1 null clones were selected. Western blot analysis of MLH1 protein levels in parental CT26 stably infected with the CRISPR construct (CT26 Cas9$^+$), CT26 *Mlh1* wild-type clone (CT26 ctrl1), and the indicated *Mlh1* KO clones. **D,** MSI assessment of the indicated clones. The mononucleotide regions AA003063 and Bat64 were used to evaluate MSI. **E,** Exome data of the indicated CT26 clones were analyzed and used to identify predicted MHC class I–specific neoantigens derived from SNVs and frameshift alterations as described in the Methods.

Tumor burden has been previously shown to affect response to PD-1 blockade in murine cancer models (31). Indeed, differently from what we observed when treating small tumors (60 mm^3), we found that anti–PD-1 treatment was ineffective when murine *B2m*-deficient MMRd tumors had reached 160 mm^3 in volume (Fig. 2C). In order to improve the efficacy of immunotherapy in larger *B2m*-deficient MMRd tumors, anti-CTLA4 was added to anti–PD-1. This combined therapeutic regimen was remarkably effective (Fig. 2C), leading to regression of large *B2m*-deficient MMRd colon tumors in several mice (Supplementary Fig. S6). To evaluate the contribution of the adaptive immune compartments in *B2m* and *Mlh1* KO tumors, we injected CT26, *B2m* KO, and *Mlh1/B2m* KO clones into mice and assessed the presence of CD3$^+$, CD4$^+$, and CD8$^+$ T cells. We noted that CD4$^+$ and CD8$^+$ T cells were more abundant in *Mlh1/B2m* KO tumors than in *B2m* KO and control CT26 (Fig. 3A). To functionally characterize the mechanism underlying the efficacy of anti–PD-1 and anti-CTLA4, we analyzed the tumor immune infiltrate in samples obtained from mice in which ICPis delayed tumor growth (Fig. 3B). We found that ICPi administration induced a remodeling of the immune infiltrate, as both CD8$^+$ and CD4$^+$ T cells were significantly increased (Fig. 3B). In addition, upon ICPi treatment, higher frequencies of both CD4$^+$ and CD8$^+$ T cells with an effector memory CD44^{hi}CD62L^{lo} phenotype were detected compared with controls (Fig. 3B). Of note, higher frequencies of infiltrating T cells under the pressure of ICPis expressed CD69, an early activation marker, and granzyme B (Fig. 3C). Concomitantly, we found that the ICPi treatment significantly reduced the frequency of PD-1$^+$ CD8$^+$ T cells, suggesting a possible reversion of an exhausted phenotype. We also investigated the relative representation of regulatory T (Treg) cells and γδ T cell populations, as these cells are known to antagonize effective anticancer immune responses and are, respectively, more greatly represented in human MMRd than in MMR-proficient tumors (32, 33). Although Treg cells were mostly unchanged, γδ T cells were significantly reduced after ICPi administration (Fig. 3C). The functional relevance of these findings remains to be defined, but these data underline the ability of ICPis to reshape the immune contexture of *Mlh1/B2m* KO tumors.

Finally, we analyzed B cells and components of the innate immune compartment due to their well-described role in cancer and ICPi responses (34, 35). In particular, no significant changes could be detected in the frequency of B cells,

Published OnlineFirst March 2, 2021; DOI: 10.1158/2159-8290.CD-20-0987

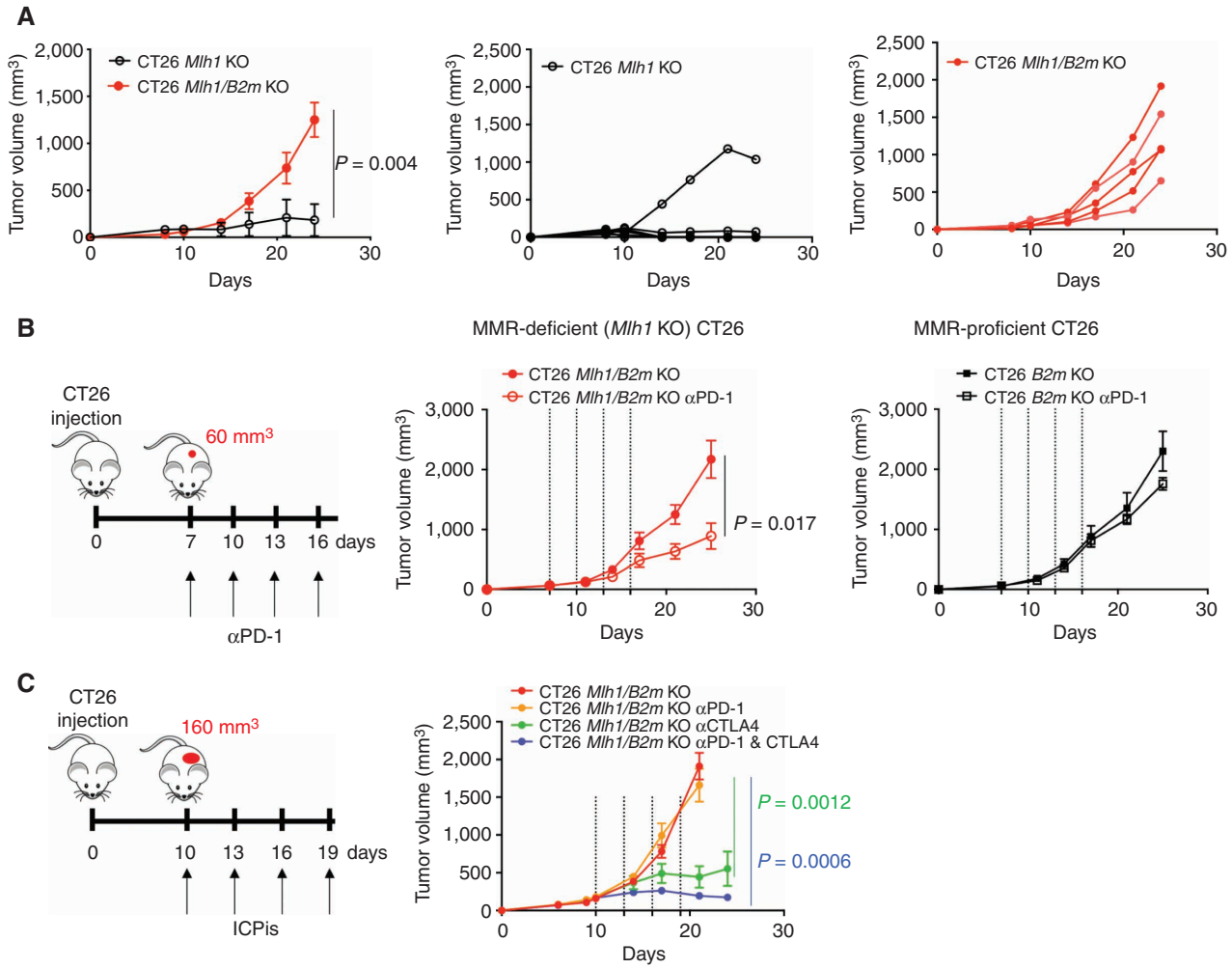

Figure 2. Functional impact of *Mlh1 and B2m* inactivation on tumor immune surveillance and response to anti-PD-1. **A,** CT26 *Mlh1* KO and *Mlh1/B2m* KO cells (5×10^5 cells per mouse) were subcutaneously (s.c.) injected into BALB/c mice. Average tumor volume (left) and individual tumor development (middle and right panels) are indicated. Loss of B2M restores tumor development of MLH1-deficient CT26. **B,** CT26 *Mlh1/B2m* KO (MMR-deficient) and CT26 *B2m* KO (MMR-proficient) cells (5×10^5 cells per mouse) were injected s.c. in BALB/c mice. After 7 days, mice were randomized and left untreated or injected intraperitoneally (i.p.) with anti-PD-1 mAb (250 μg/mouse) every three days for four times in total. The experiments were performed twice. **C,** CT26 *Mlh1/B2m* KO cells were injected s.c. (5×10^5 cells per mouse) in BALB/c mice. After 10 days, when the size of tumors was between 150 and 200 mm^3, anti-PD-1 (250 μg per mouse) and anti-CTLA4 (200 μg per mouse) antibodies were administered i.p. individually or in combination. Antibody administrations were repeated every 3 days for four times in total. Tumor growth was measured and average tumor volume ± SEM is indicated. Every experimental group was composed at least of six mice. Dotted lines indicate the days of combinatorial treatment. The experiment was performed once for single anti-PD-1 and anti-CTLA4 treatments and twice for the combination (one of which is shown). *P* values were calculated by the Mann–Whitney non-parametric test.

macrophages, $CD11c^+$ MHC class II–positive dendritic cells, neutrophils, and monocytes comparing untreated and ICPi-treated tumors (Supplementary Fig. S7). We instead found a reduction in the frequency of natural killer (NK) cells.

To expand the above findings beyond colorectal tumors, MMRd PDAC cells, lacking B2M, were treated with anti–PD-1 and anti-CTLA4 mAb injected individually or together. We found that anti–PD-1 monotherapy treatment moderately delayed tumor growth, whereas anti–PD-1 combined with anti-CTLA4 greatly improved PDAC cell rejection (Fig. 4A; Supplementary Fig. S8). The effect of combinatorial anti–PD-1 and anti-CTLA4 treatment on tumor regression was dependent on MMR status in PDAC tumor models. The same treatment was ineffective on the isogenic MMR-proficient counterpart (Fig. 4B).

We reasoned that *B2m* deficiency could influence tumor growth via non-immune mechanisms. To assess this possibility, double (*Mlh1/B2m*) KO PDAC cells were also injected into immunocompromised—nonobese diabetic (NOD)/severe combined immunodeficiency (SCID)—animals that then received anti–PD-1 and anti-CTLA4 antibodies. In the absence of a functional adaptive immune system, the combinatorial treatment did not affect the growth of *Mlh1/B2m* KO tumors (Fig. 4C). To assess whether combinatorial treatment could be broadly effective on other MMRd tumors types with defective APM, immune-competent mice were injected with *Mlh1/B2m*

Published OnlineFirst March 2, 2021; DOI: 10.1158/2159-8290.CD-20-0987

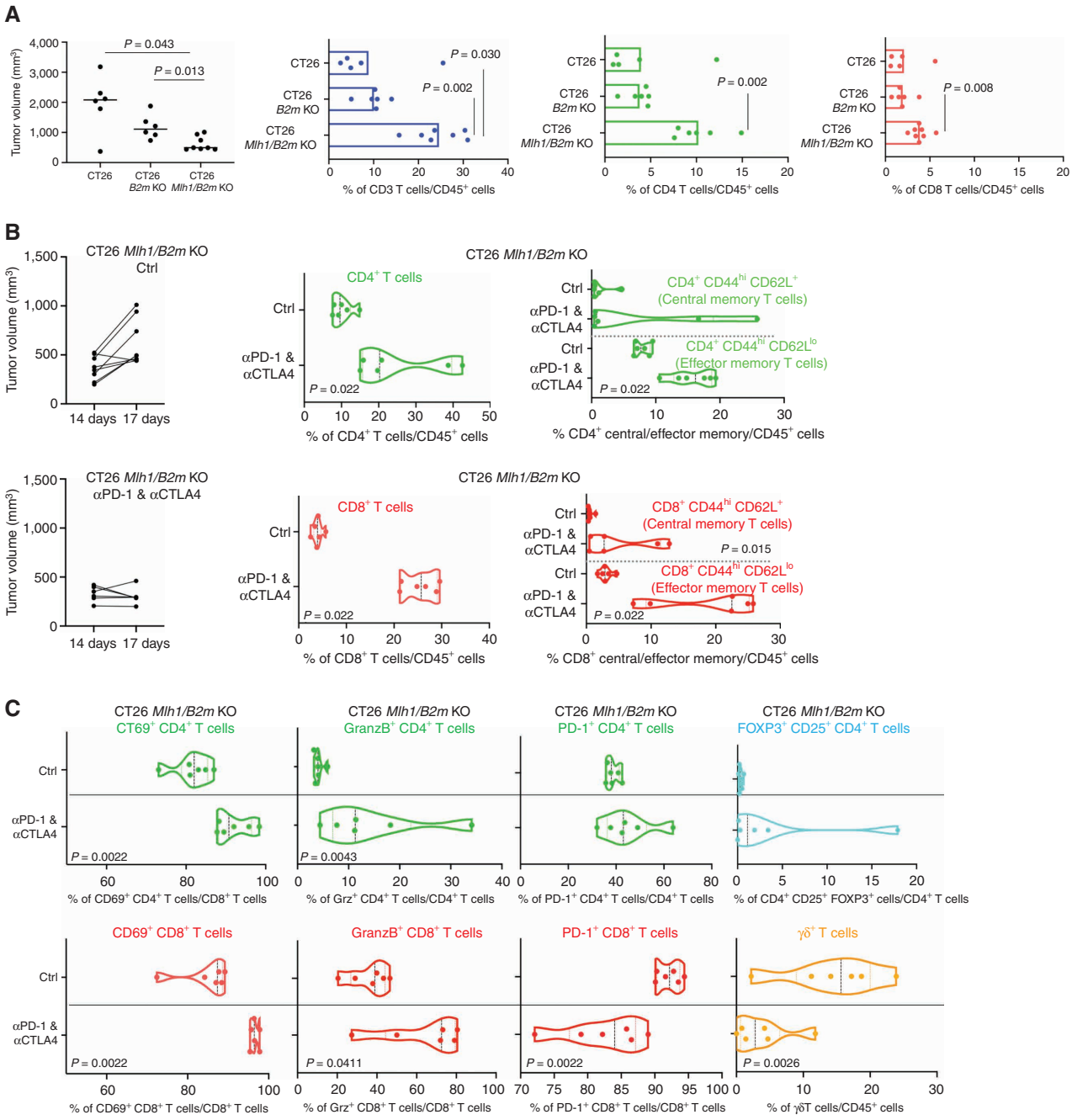

Figure 3. Effect of immune checkpoint blockades on the microenvironment of tumors lacking *B2m*. **A,** CT26 (control clone), CT26 *B2m* KO, and *Mlh1/B2m* KO cells were injected s.c. (5×10^5 cells per mouse) in immune-competent BALB/c mice which were sacrificed at day 17, and then the tumors were recovered. The immune infiltrate was evaluated by FACS. The events of $CD3^+$, $CD4^+$, and $CD8^+$ T cells were gated within $CD45^+$ live cells. **B,** In the same experiment described in **A**, mice bearing CT26 *Mlh1/B2m* KO cells were treated i.p. with anti-PD-1 (250 μg per mouse) and anti-CTLA4 (200 μg per mouse) antibodies. Mice were sacrificed after three doses of ICPi (17 days after injection). The percentages of $CD4^+$ and $CD8^+$ T cells were evaluated within live $CD45^+$ cells. In addition, central memory ($CD44^{hi}CD62L^+$) and effector memory ($CD44^{hi}CD62L^-$) phenotypes were estimated. **C,** In the same experiment described in **B**, $CD69^+$, granzyme B^+, and $PD\text{-}1^+$ cells were determined within $CD4^+$ T cells (top) and $CD8^+$ T cells (bottom). Treg cells ($CD45^+$ $CD3^+$ $CD4^+$ $CD25^+$ $FOXP3^+$) and γδ T cells ($CD45^+$ $CD3^+$ γδTCR$^+$) were also estimated in the tumor microenvironment. Every experimental group was composed at least of six mice. The experiment was performed twice with similar results. *P* values were calculated by Mann–Whitney non-parametric test.

Published OnlineFirst March 2, 2021; DOI: 10.1158/2159-8290.CD-20-0987

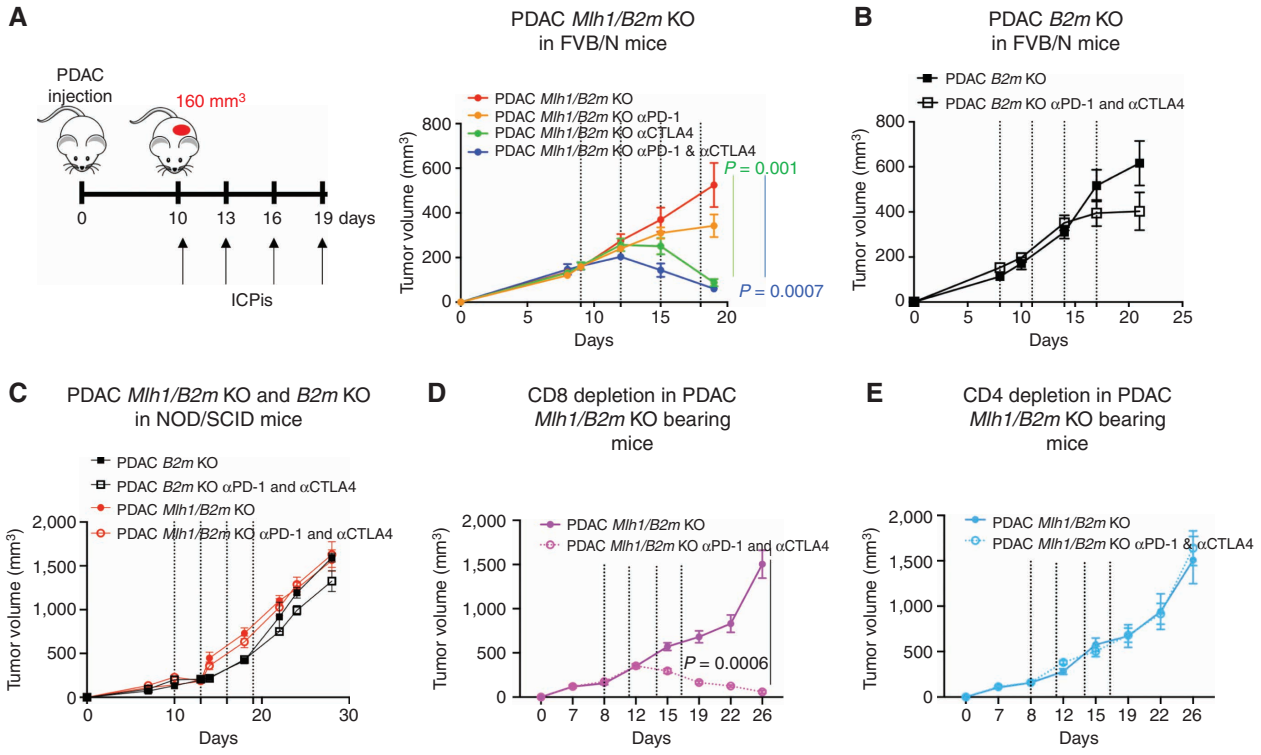

Figure 4. Functional impact of immune cell populations on the growth of *Mlh1/B2m* KO pancreatic tumors. **A,** PDAC *Mlh1/B2m* KO cells were injected (5×10^5 cells per mouse) s.c. in syngeneic FVB/N mice. When tumor volumes reached 160 mm^3, mice were randomized and treated with anti–PD-1 (250 μg per mouse) and anti-CTLA4 (200 μg per mouse) alone or in combination. Antibody administration was repeated every 3 days for four times in total. **B,** PDAC *B2m* KO cells were injected and treated as described in **A**. **C,** PDAC cells were injected subcutaneously (5×10^5 cells per mouse) in NOD/SCID immune-compromised mice. Mice were randomized between 150 mm^3 and 200 mm^3 and divided into two groups (ctrl and combo treatment). Anti–PD-1 and anti-CTLA4 antibodies were administered as described in **A**. **D** and **E,** PDAC *Mlh1/B2m* KO tumors were injected in immune-competent mice as described in **A**. Mice were treated with anti–PD-1 and anti-CTLA4 antibodies when tumor size was between 150 mm^3 and 200 mm^3. Blocking antibodies against CD8$^+$ T cells (**D**) and CD4$^+$ T cells (**E**) were administered at the day of tumor injection, the second day, and then every third day after tumor injection. Experimental groups were composed at least of six mice. The experiments were performed once with the exception of the experiment represented in **A** which was performed twice for the anti–PD-1 and anti-CTLA4 antibody combined group. Dotted lines indicate the days of anti–PD-1 and anti-CTLA4 antibody treatments. Data and error bars indicate mean ± SEM. *P* values were calculated by Mann–Whitney nonparametric test.

KO TS/A breast cancer cells and treated with anti–PD-1 and anti-CTLA4 when tumors had reached 200 mm^3. Combinatorial treatment also strongly impaired tumor growth in the breast cancer model (Supplementary Fig. S9A and S9B).

CD4$^+$ T Cells Are Required for ICPi Efficacy against *B2m*-Deficient MMRd Tumors

Because both CD8$^+$ and CD4$^+$ T cells were significantly increased in *Mlh1/B2m* KO tumors treated with ICPis, we investigated their relative contribution to immune surveillance. To this aim, mice with *Mlh1/B2m* KO PDAC tumors were treated with anti–CD8- and anti–CD4-depleting antibodies. Depletion was confirmed by flow cytometric analysis of peripheral blood (Supplementary Fig. S10A–S10C). Although depleting CD8$^+$ T cells did not impair the efficacy of the ICPis (Fig. 4D), the absence of peripheral CD4$^+$ T cells rendered tumors insensitive to the combined anti-CTLA4 and anti–PD-1 treatment (Fig. 4E). The contribution of CD4$^+$ T cells was also evaluated in the colorectal cancer model. Notably, depleting CD4$^+$ T cells (Supplementary Fig. S11A), but not CD8$^+$ T cells (Supplementary Fig. S11B), abolished the efficacy of the combined anti–PD-1 and anti-CTLA4 treatment. These data support the notion that CD4$^+$ T cells modulate responsiveness of *B2m*-deficient MMRd tumors to immune checkpoint blockade.

CD4$^+$ T cells have been shown to mediate anticancer immune responses indirectly via the activation of antigen-presenting cells or through direct binding to MHC class II–positive tumor cells (36). To test the impact of *B2m* deficiency on MHC class II status, we measured the surface levels of MHC class II in CT26, PDAC, and TS/A cells upon stimulation with IFNγ (Supplementary Fig. S12A). All of the cell lines tested were negative for MHC class II after stimulation with IFNγ. However, the number of MHC class II–positive cells increased in *Mlh1/B2m* KO CT26 tumors after *in vivo* treatment with anti–PD-1 and anti-CTLA4 (Supplementary Fig. S12B).

Finally, the contribution of CD4$^+$ T cells was also evaluated in CT26 tumors after anti–PD-1 treatment alone. Intriguingly, we noted that CD4$^+$ T-cell depletion compromised the efficacy of anti–PD-1 as monotherapy in the colorectal cancer model (Supplementary Fig. S13A and S13B). Considering the effectiveness of pembrolizumab in patients with MSI colorectal cancer, these findings highlight the role of CD4$^+$ T cells in response to anti–PD-1.

Published OnlineFirst March 2, 2021; DOI: 10.1158/2159-8290.CD-20-0987

Patients with MMRd Tumors Frequently Harbor Inactivating Mutations in *B2M* and Other Genes Involved in Antigen Presentation but Still Respond to Immune Checkpoint Blockade

To establish the relevance of the above findings in human cancer and inform treatment of patients bearing MMRd tumors, six cohorts of patients with colorectal, endometrial, esophageal, and stomach cancers were stratified based on the total number of tumor somatic mutations, microsatellite stable (MSS)/MSI and *POLE* status, and alterations in the APM (e.g., *B2M, TAP1, TAP2,* Calreticulin, Calnexin, *TAPBP*, *HLA*; Fig. 5A). Genomic data from The Cancer Genome Atlas (TCGA), Dana-Farber Cancer Institute (DFCI), and Memorial Sloan Kettering (MSK) cohorts were downloaded from cBioportal (37, 38). Truncating and missense driver mutations, as well as copy-number deletions in the APM, were enriched in hypermutated and MSI tumors. To assess whether this enhancement was specific and not due to the hypermutability of MSI tumors, we selected nine random genes with base-pair lengths analogous to those of the APM genes. Next, we performed a simulation analysis to evaluate the average number of mutations in the random gene set in the same tumors. The frequency of alterations in the APM set in hypermutated cancers was significantly increased compared with the controls (Spearman correlation coefficient = 0.08, $P < 0.00042$). These data indicate that, in MSI cancers, the occurrence of deleterious events effecting APM genes is driven by a selective process and not by random alterations associated with the hypermutated status. To further explore the clinical relevance of *B2M* loss in MSI malignancies, we examined whole-exome sequencing on pretreatment tissues from a cohort of patients with MMRd tumors treated with pembrolizumab. We identified three patients (with colorectal, duodenal, and endometrial cancer, respectively) who had frameshift mutations in *B2M* with loss of heterozygosity (LOH) events at its locus on chromosome 15 (Fig. 5B), suggesting biallelic loss of *B2M* and that had received immunotherapy treatment. Interestingly, all three cases showed radiographic responses to anti–PD-1 monotherapy (Fig. 5B and C). In patients with *B2M*-mutant tumors, we examined both total mutation burden and the total number of frameshift mutations to ensure that the observed response to anti–PD-1 was not attributable simply to a difference in the general genomic background, and we found no differences (Fig. 5D, E).

Next, we evaluated the outcome of anti–PD-1 treatment in a cohort of 38 patients bearing MSI tumors; a majority of the patients had colorectal cancer, but other tumor types included endometrial and pancreatic cancers. They were classified for B2M expression as measured by multiplex immunofluorescence (mIF). Interestingly, levels of B2M expression did not affect overall survival (OS) or progression-free survival (PFS; Fig. 6A, B), indicating that MSI tumors remain responsive to ICPis despite genetic alterations in MHC class I antigen presentation. Comparable results were obtained correlating survival with MHC class I levels (Supplementary Fig. S14).

MMRd Cancers with Low Levels of B2M Are Infiltrated by Both $CD8^+$ and $CD3^+CD8^-$ T Cells

Next, we used RNA sequencing (RNA-seq) and mIF to study the immune cell composition in tumor sections from patients with MMRd cancer treated with PD-1 blockade. Of the immune compartments analyzed by CIBERSORT (39, 40), only $CD4^+$ T cells (memory-activated, memory-resting, and naïve T cells) had a statistically significant negative correlation with B2M expression (Fig. 6C). This relationship was also reflected by mIF, as $CD3^+CD8^-$ cell densities were higher in tumors expressing lower levels of B2M, despite the low number of patients analyzed (Supplementary Fig. S15A). Interestingly, we also noted an increase in the staining of $CD3^+$ and $CD8^+$ cells in samples expressing low levels of B2M as compared with samples expressing high levels of B2M (Supplementary Fig. S15A). It has previously been shown that activated $CD4^+$ T cells express high levels of PD-L1 (41). We found more infiltrating $PD\text{-}L1^+CD3^+CD8^-$ cells in MSI tumors that expressed lower levels of B2M, confirming a role for $CD4^+$ T cells as well in the immune response against MMRd tumors in the context of low B2M expression (Supplementary Fig. S15B). Of note, $CD3^+$, $CD8^+$, and $CD3^+CD8^-$ cells expressing PD-L1 were similarly enriched in tumors expressing low levels of B2M (Supplementary Fig. S15B), supporting intratumoral activation (42) and responsiveness to ICPis. Overall, these results indicate that MMRd tumors remain responsive to ICPis, regardless of the expression of B2M, and they pinpoint $CD4^+$ T cells as potential drivers in instructing protective immunity in this clinical setting.

DISCUSSION

Molecular defects of genes involved in antigen presentation are a purported mechanism of clinical resistance to ICPis in melanoma and lung tumors (12, 43). A previous study reported that the knockout of *B2m* confers resistance to anti–PD-1 treatment in a mouse model of lung cancer (12), and, similarly, resistance to anti–PD-1 blockade was observed when *B2m* was genetically ablated in the chemically induced murine MC38 colon carcinoma model (44), which has a high mutational burden but does not display alterations in MMR genes (8). On the other hand, a clinical study has reported that the absence of a functional APM does not prevent response to immune checkpoint blockade in patients with MMRd cancer (24). Whether this is a general phenomenon occurring in MSI tumors and the functional basis for ICPi efficacy in MSI tumors with alterations in *B2M* remain to be clarified. In this study, we therefore characterized the significance of *B2m* loss-of-function mutations to gain mechanistic insights into the role of antigen presentation in the context of MSI cancers treated with ICPis.

We had previously found that MMRd colon cancer, breast cancer, and PDAC cells are unable to effectively form tumors in immune-competent mice (8). In this work, we report that *B2m* loss fully rescues the tumorigenicity of MMRd cells in immune-competent animals. In agreement with previous studies (12, 44), we found that the absence of B2M leads to the loss of surface MHC class I expression, which is known to hinder the functionality of the MHC class I–T-cell receptor complex and consequently alters tumor control by T cells. Our data therefore suggest that class I antigen presentation and $CD8^+$ T cells are pivotal to triggering immune surveillance of MMRd tumors. These findings also further support loss of *B2m* as a central mechanism by which cancer cells

Published OnlineFirst March 2, 2021; DOI: 10.1158/2159-8290.CD-20-0987

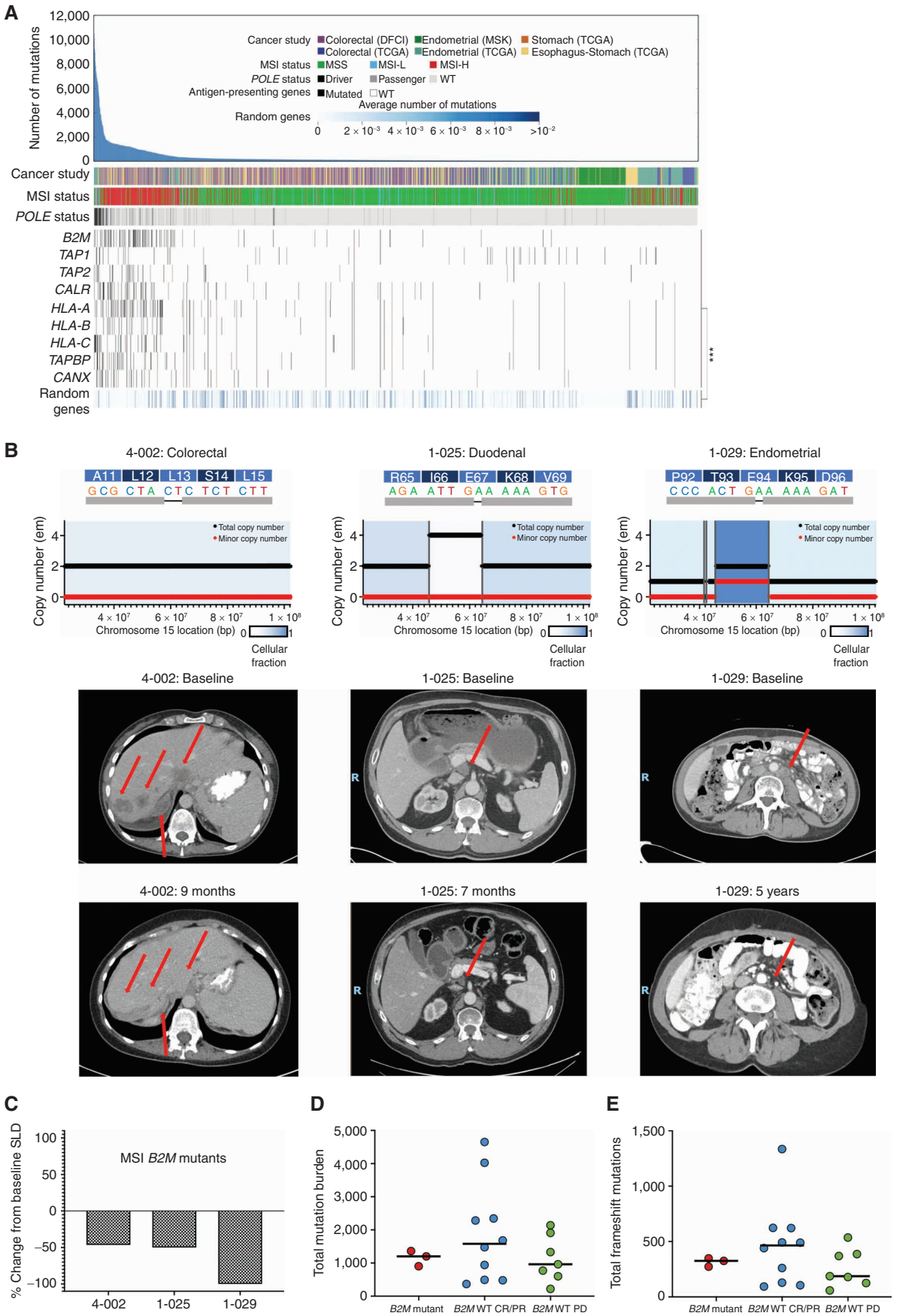

Published OnlineFirst March 2, 2021; DOI: 10.1158/2159-8290.CD-20-0987

escape immune control in highly neoantigenic tumors such as those with MMR deficiency.

CD8$^+$ T cells appear crucial in controlling the growth of B2M-proficient MMRd tumors, and relatively small B2M-deficient MMRd murine cancers remained sensitive to anti–PD-1 monotherapy, suggesting preserved immune-mediated control. Intriguingly, although anti–PD-1 alone was ineffective in restraining the growth of larger *B2m*-defective MMRd cancers, its combination with anti-CTLA4 was able to induce disease regression in mice. In mouse models, combined anti-CTLA4 and anti–PD-1 treatment is required to achieve maximal antitumor efficacy, whereas patients with *B2M*-deficient MSI colorectal cancer have been reported to respond to anti–PD-1 alone (24). Although evolutionary differences might account for this discrepancy, our data suggest that combined anti-CTLA4 and anti–PD-1 treatment could lead to improved efficacy in patients with MSI tumors and concomitant *B2M* inactivation or other defects in the APM. This possibility could be readily tested in the clinical setting.

Analysis of the tumor microenvironment and functional assays in mouse models revealed that CD4$^+$ T cells are pivotal in establishing an effective cancer immune response once stimulated by anti-CTLA4 and anti–PD-1, but only in the context of MMRd tumors. Notably, double *Mlh1/B2m* KO tumors treated with combination ICPis displayed increased fractions of both CD4$^+$ and CD8$^+$ T cells. Additionally, the percentages of memory effector CD4$^+$ and CD8$^+$ T cells were higher and CD69$^+$ and granzyme B$^+$ T cells were specifically enriched after anti–PD-1 and anti-CTLA4. To investigate cell-mediated mechanisms of antitumor immunity, we selectively depleted CD8$^+$ or CD4$^+$ T cells in PDAC and colorectal cancer preclinical models. Although CD8$^+$ T cells showed an activated phenotype and might provide bystander killing activity (45), their depletion did not affect tumor growth upon ICPi treatment. In contrast, immune depletion of peripheral CD4$^+$ T cells rendered combinatorial treatment with anti-CTLA4 and anti–PD-1 largely ineffective.

The finding that MSI murine tumors remain responsive to ICPis in a CD4$^+$ T cell–dependent manner could be relevant for human disease. CD4$^+$ T cells might favor tumor eradication via several mechanisms. One possibility is that CD4$^+$ T cells may eliminate MHC class II–negative tumors by IFNγ without involvement of CD8$^+$ T cells (46). Another possibility is that *Mlh1* deletion could lead to expression of MHC class II–restricted neoantigens. These might be cross-presented by professional antigen-presenting cells and result in better priming and tumor infiltration by effector CD4$^+$ T helper cells.

Although the vast majority of tumors do not express MHC class II, we cannot exclude the possibility that, in the MMRd tumors described here, MHC class II–restricted neoantigens might at least partially support immune responses. None of the cell lines we studied expressed MHC class II; however, in CT26 *Mlh1/B2m* KO tumors the *in vivo* administration of ICPis increased the percentage of MHC class II–positive cells. Finally, CD4$^+$ T cells could exert a non–MHC-restricted tumor control, independently from T-cell receptor activation and mediated by cytokine release (47).

We speculate that anti-CTLA4 and anti–PD-1 antibodies could favor CD4$^+$ T cell priming in secondary lymphoid organs and enhance antitumor effects within the tumor, respectively. In particular, anti–PD-1 antibodies could favor T-helper cell (Th)1 (rather than Th17) cell commitment and promote CD4$^+$ T-dependent M1-tumor–associated macrophage differentiation (rather than M2). CD4-stimulated M1 cells might in turn exert killing activity via the secretion of nitric oxide (48). In addition, CD4$^+$ T cells could promote activation of myeloid cells, especially CD103$^+$ dendritic cells (49), which might drive NK cell recruitment and activation via IL12 production. Although the relevance of NK cells in MSI tumors lacking B2M remains to be further explored, the findings that NK cells partially impair tumor regression in *B2m* KO tumors is suggestive of their involvement in tumor eradication (13, 50, 51). However, the functional implications of MHC class I–mediated NK modulation are still debated; for example, recently the laboratories of Poursine-Laurent and Yokoyama (52) reported that down-modulation of MHC class I can induce either NK-cell tolerance or killing *in vivo*. Nevertheless, we acknowledge that the mechanisms by which CD4$^+$ T cells mediate efficient anticancer immune responses in double *Mlh1/B2m* KO tumors treated with combination ICPis remain to be fully clarified, and future studies should address this remaining issue.

The majority of patients with *B2M*-mutant MSI colorectal cancer show clinical benefit from treatment with ICPis (24). In this work, we provide initial evidence that patients bearing MMRd cancers other than colorectal cancer (such

Figure 5. Mutations in APM genes are enriched in hypermutated tumors, but *B2M* alterations do not preclude response to anti–PD-1 in patients with MSI cancer. **A,** Mutations in antigen–presenting genes are enriched in hypermutated tumors. Data on patients with colorectal, endometrial, stomach, or esophageal cancer were collected from the TCGA, MSK, and DFCI databases. The mutation landscape of antigen-presenting genes in 1,845 tumor samples is represented. Samples were sorted by number of mutations (SNVs, indels, and copy-number deletion) and classified for MSI and *POLE* status. Patients with *POLE* alterations were classified using the oncoKB annotation (driver and passenger alterations). Random genes values represent the average value of mutations across 100 random gene sets having lengths comparable to those of the antigen-presenting genes. $P = 0.00042$ for Spearman non-correlation between the average of the mutations in random genes and in the antigen-presenting genes. **B,** Clinical response to ICPi of patients with cancer with tumors carrying alterations in *B2M*. *B2M* mutations resulting in frameshift and LOH events at the *B2M* locus determined by FACETS are indicated for each patient. Total and minor copy-number calls are plotted with corresponding estimated cellular fraction profiles. For each patient, the baseline radiographic scan is shown alongside the scan at the time point of the patient's best objective response as determined by RECIST 1.1. **C,** Waterfall plot of radiographic response with the best fractional change of the sum of longest diameters (SLD) from the baseline measurements of each measurable tumor. **D,** Tumor mutation burden of *B2M*-mutant patients as compared with other MSI patients ($n = 17$). **E,** Total number of frameshift mutations in *B2M*-mutant patients in relation to other MSI patients. In **D** and **E**, the following cancer types were included: endometrial, gastroesophageal, colorectal, small intestine, and ampullary. WT, wild-type; CR, complete response; PR, partial response; PD, progressive disease.

Published OnlineFirst March 2, 2021; DOI: 10.1158/2159-8290.CD-20-0987

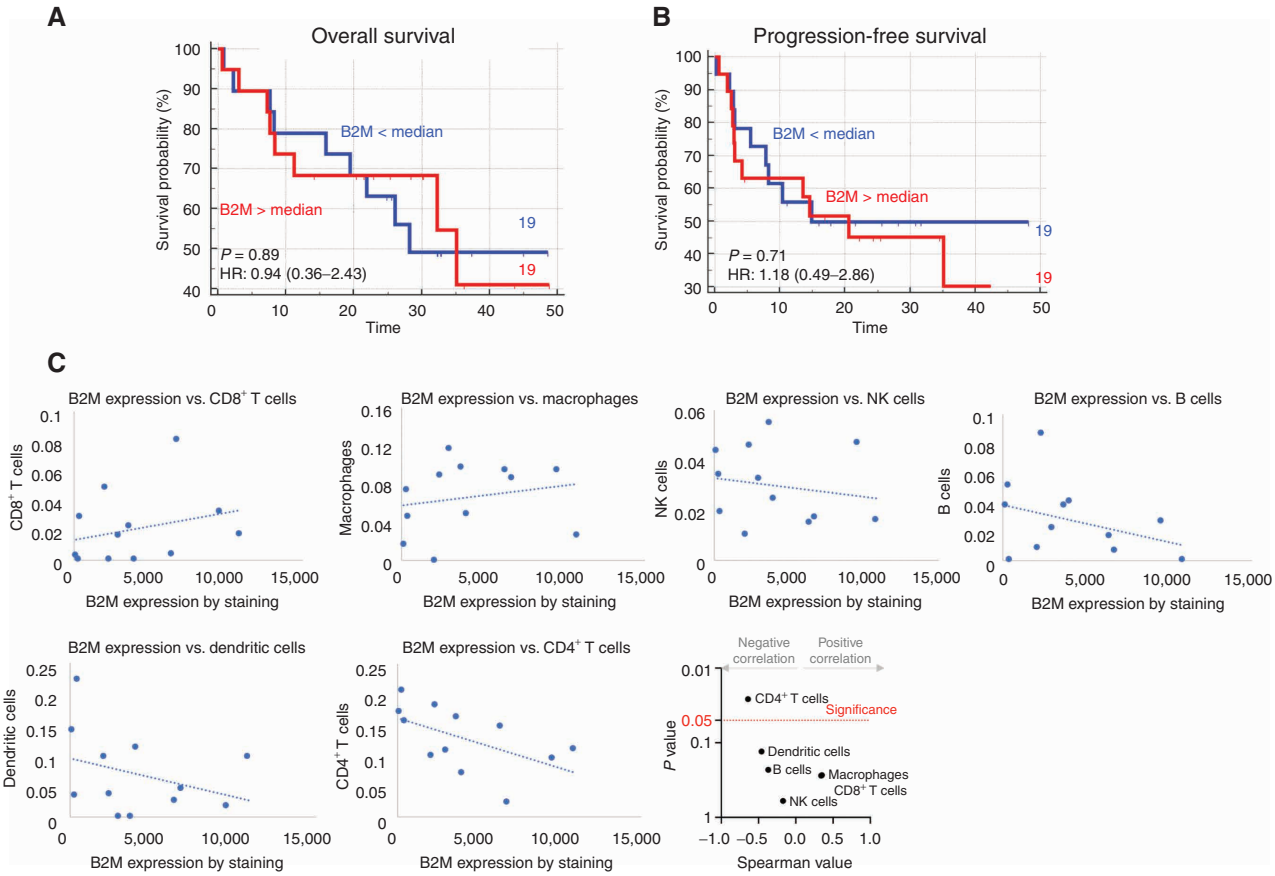

Figure 6. Upon anti–PD-1 treatment, MSI patients bearing low B2M–expressing tumors showed similar PFS or OS compared with those with higher B2M expression; low B2M–expressing tumors correlate negatively with CD4+ T cell density. **A** and **B,** Kaplan–Meier OS (**A**) and PFS (**B**) curves for MMRd patients treated with anti–PD-1 and classified according to levels of B2M expression above (red) and below (blue) the median. *P* values and hazard ratios (HR) are shown. In **A** and **B,** the following cancer types were included in the cohorts: endometrial, gastroesophageal, colorectal, small intestine, and pancreatic cancer, as well as cholangiocarcinoma. **C,** The association between immune cell infiltrates and B2M expression was assessed in MSI tumors by CIBERSORT. The abundance of CD8+ and CD4+ T cells, NK cells, B cells, and dendritic cells were correlated with B2M expression. Endometrial, colorectal, and duodenal cancers were included in the cohort. Spearman and *P* values were calculated and are shown on the bottom right part of panel **C**.

as duodenal and endometrial cancer) may receive benefit from ICPis. We also show that patients bearing MSI tumors achieve a survival benefit with anti–PD-1 treatment irrespective of B2M expression levels. Finally, we found that tumors treated with anti–PD-1 with low expression of B2M contained greater numbers of CD4+ T cells. These findings are supported by preclinical data, as CD4+ T-cell depletion has been shown to abolish the effectiveness of single anti–PD-1 treatment in colorectal cancer. Thus, CD4+ T cells appear to mediate rejection of MSI tumors lacking HLA class I antigen presentation.

In conclusion, our work highlights the role of tumor-associated effector CD4+ T cells in preclinical models and patients with impaired APM. As CD4+ T cells have the ability to orchestrate a wide range of immune responses, their role is becoming highly relevant in immunotherapy. We therefore emphasize that, in some tumor types, CD4-mediated tumor rejection could be more effective than that of CD8+ T cells (53). Intriguingly, in infectious diseases (54) when the MHC class I–T-cell receptor axis is compromised, other immune compartments exert the cytotoxic function of CD8+ T cells. Conceptually, similar mechanisms might have been developed to restrict tumor growth.

METHODS

Cell Models

CT26 is a mouse-undifferentiated colon carcinoma derived from BALB/c and was obtained from the ATCC. The TS/A breast cancer cell line was established from a moderately differentiated mammary adenocarcinoma that arose spontaneously in a BALB/c mouse (55). TS/A cells were kindly provided by Federica Cavallo (Molecular Biotechnology Center, University of Torino, Italy). Murine PDAC cells were isolated, as previously described (56), from transgenic mice bearing pancreatic cancers with the following genotype: *p48*^{cre}, *Kras*$^{LSL\_G12D}$, *Trp53*$^{R172H/+}$, *Ink4a/Arf*$^{flox/+}$. PDAC cells were kindly provided by Doug Hanahan (Swiss Institute for Experimental Cancer Research, EPFL, Lausanne, Switzerland; ref. 57). CT26 cells were cultured in RPMI 1640 10% FBS plus glutamine, penicillin, and streptomycin (Sigma-Aldrich). TS/A and PDAC cells were cultured in high-glucose DMEM and 10% FBS

Published OnlineFirst March 2, 2021; DOI: 10.1158/2159-8290.CD-20-0987

plus glutamine, penicillin, and streptomycin (Sigma-Aldrich). All of the cell lines were exome-sequenced before initiating the project to confirm identity. To ensure that the parental cell models were tumorigenic, before we began the genome-editing experiments, the lines were injected in matched syngeneic mice. Upon tumor formation, we reestablished *in vitro* cell cultures. All cell lines were tested for *Mycoplasma* regularly.

Animal Studies

All animal procedures were approved by the Ethical Commission of the University of Turin and by the Italian Ministry of Health and were performed in accordance with institutional guidelines (4D.L.N.116, G.U., suppl. 40, 18-2-1992) and international law and policies (EEC Council Directive 86/609, OJ L 358, 1, 12 December 1987; 1996 National Institutes of Health Guide for the Care and Use of Laboratory Animals). The number of mice included in the experiments and the inclusion/exclusion criteria were based on institutional guidelines (above). Our protocol limited us to using 6- to 8-week-old female and male BALB/c, FVB/N, and NOD/SCID mice. Mice were obtained from Charles River Laboratories Italia. All experiments involved a minimum of five mice per group. Tumor size was calculated using the formula: $V = [(d/2)^2 \times (D/2)]/2$, where d = minor tumor axis, and D = major tumor axis, and reported as tumor mass volume (mm^3, mean ± SEM of individual tumor volume). The investigators were not blinded. Animals were examined by veterinary personnel during the entire duration of the experiments. Mice were monitored at least three times a week for social behaviors (such as grooming and nursing), signs of illness, and reduced and/or impaired motility. Mice were housed in individually ventilated cages in a pathogen-free animal facility. No statistical methods were used to predetermine sample size.

Gene Editing

To knockout the *Mlh1* and *B2m* genes in mouse cells we used the genome editing one vector system (lentiCRISPR-v2, 52961; Addgene) as previously reported (8). Briefly, single-guide RNAs (sgRNA) were designed using the CRISPR tool (http://crispr.mit.edu) to minimize potential off-target effects. For transient expression of the CRISPR/Cas9 system, we transfected cells with lentiCRISPR-v2 vector plasmid (same guides as previously described). Transfection was carried out using Lipofectamine 3000 (Life Technologies) and Opti-MEM (Invitrogen), according to the manufacturers' instructions. After 48 hours, cells were incubated with puromycin (Sigma-Aldrich) for 2 days, and subsequently single-cell dilution was performed in 96-well plates. The absence of MLH1, B2M, and Cas9 was confirmed by Western blot.

MSI Analysis

MSI in mouse cells was determined using a panel of three microsatellite markers as previously described (58). Amplification was performed with the following primers: fluorescein mBat64, forward GCCCACACTCCTGAAAACAGTCAT and reverse CCCTGGT GTGGCAACTTTAAGC; AC096777 JOE, forward TCCCTGTATA ACCCTGGCTGACT and reverse GCAACCAGTTGTCCTGGCGTGGA; AA003063 Tamra, forward ACGTCAAAAATCAATGTTAGG and reverse CAGCAAGGGTCCCTGTCTTA; and U12235 JOE, forward GCTCATCTTCGTTCCCTGTC and reverse CATTCGGTGGAAAGCT CTGA. Polymerase chain reaction (PCR) was performed in 20 μL of PCR reaction using the Invitrogen Platinum Taq DNA Polymerase Kit and 20 ng of DNA. The cycling profile was one cycle of 94°C for 4 minutes, then 35 cycles of 94°C for 30 seconds, 56°C for 45 seconds, and 72°C for 30 seconds. A final extension at 72°C for 6 minutes completed the amplification. PCR fragments were separated on a 3730 DNA analyzer (Applied Biosystems), and raw data were analyzed with GeneMapper software.

Mouse Treatments

The anti-mouse PD-1 (clone RMP1-14), anti-mouse CTLA4 (clone 9H10), anti-mouse CD8a (YTS169.4), and anti-mouse CD4 (clone GK1.5) were purchased from Bio X Cell. Randomization was used for the experiments where therapeutic effects had to be evaluated (e.g., anti–PD-1 and anti-CTLA4). Mice were treated intraperitoneally (i.p.) with 250 μg per mouse of anti–PD-1 and 200 μg per mouse of anti-CTLA4. Treatments were initiated when tumor size was between 150 and 200 mm^3, with the exception of the experiment in Fig. 2B and in Supplementary Fig. S13 (as indicated in the figure legend). Anti–PD-1 was given every 3 days. Anti-mouse CD4 (clone GK1.5) and CD8a (clone YTS169.4) were used for depleting T cells in immune-competent mice. Anti-mouse CD4, anti-CD8a antibody (400 μg per mouse) were administered i.p. the same day of tumor injection. In addition, 2 days after tumor injection and then every 3 days mice were treated with blocking antibodies.

Western Blot Analysis

For biochemical analysis, cells were grown in media supplemented with 10% FBS. Total cellular proteins were extracted by solubilizing the cells in boiling SDS buffer (50 mmol/L Tris-HCl, pH 7.5; 150 mmol/L NaCl; and 1% SDS). Samples were boiled for 10 minutes and sonicated for 30 seconds. Extracts were clarified by centrifugation, and the amounts of proteins were normalized with the BCA Protein Assay Kit (Thermo Fisher Scientific). Western blot detection was performed with the GE Healthcare enhanced chemiluminescence system and peroxidase-conjugated secondary antibodies (Amersham). The following primary antibodies were used for Western blotting: anti-mMLH1 (epr3894; Abcam), anti-actin (I-19; Santa Cruz Biotechnology), anti-Cas9 (7A9; GeneTex), and anti-B2M (clone EP2978Y; Abcam).

Immunophenotypic Cell Analysis

Mouse tumors were cut into small pieces and disaggregated using the Tumor Dissociation Kit, mouse (Miltenyi Biotec). During the enzymatic digestion, the BD GolgiPlug protein transport inhibitor (BD Biosciences) was added into the tubes. Flow cytometry was performed using a Dako FACS instrument, Attune NxT flow cytometer (Thermo Fisher Scientific), and the BD FACSymphony (BD Biosciences). The analysis was performed using Summit 4.2 from Dako, Kaluza software from Beckman Coulter, and FlowJo. Phenotypic analysis was performed with the following antibodies purchased from Becton Dickinson: PE-Cy7 Rat Anti-Mouse CD45 (clone 30-F11), BB700 Anti-Mouse CD3e (clone 145-2C11), BV786 Rat Anti-Mouse CD4 (clone RM4-5), APC Anti-Mouse CD8a (clone 53-6.7), BB515 Rat Anti-Human/Mouse CD11b (clone M1/70), BV480 Anti-Mouse CD69 (clone H1.2F3), BV650 Anti-Mouse CD279 (clone J43), BV711 Anti Mouse IFNγ (clone XMG1.2), PE Mouse Anti-Human Granzyme B, BV605 Rat Anti-Mouse CD62 L (clone MEL14), APC-R700 Rat Anti-Mouse CD44 (clone IM7), BV421 Rat Anti-Mouse CD25 (clone PC61), PE-CF594 Anti-Mouse FOXP3 (clone MF23), BV480 Hamster Anti-Mouse CD49 (clone HMα2), BV421 Hamster Anti-Mouse γδ T-Cell Receptor (clone GL3), APC-R700 Rat Anti-Mouse CD19 (clone 1D3), BV480 Rat Anti-Mouse CD45R/B220 (clone RA3-6B2), and APC-H7 LIVE/DEAD Fixable Viability Stain 780.

The following antibodies were purchased from Biolegend: PerCp anti-mouse CD45 (clone 30-F11), APC Anti-Mouse/Human CD11b (clone M1/70), FITC Anti-Mouse CD4 (clone RM4-5), PE Anti-Mouse CD8b (clone YTS156.7.7), PE Mouse IgG2a, κ isotype (clone MOPC-173), PE Anti-Mouse H-2Kb/H-2Db (clone 28-8-6), Alexa Fluor 488 IgG2B (clone RTK4530), Alexa Fluor 488 Anti-Mouse I-A/I-E (clone M5/114.15.2), and the Zombie Violet Fixable Viability Kit.

Published OnlineFirst March 2, 2021; DOI: 10.1158/2159-8290.CD-20-0987

Mutational Loads and Neoantigen Prediction Analysis in Cell Lines

Genomic DNA of cell lines was extracted using the ReliaPrep gDNA Tissue Miniprep System (Promega), and whole-exome sequencing (WES) was performed on the Illumina HiSeq400 as paired-end 75 (PDAC and TS/A) and on Illumina NovaSeq as paired-end 100 (CT26) at IntegraGen. Raw data provided by IntegraGen were analyzed at our institution using a bioinformatics pipeline previously published (59). On average, we observed more than 98% of the targeted region covered by at least one read, and we reached a median depth of 65× for PDAC, 63× for TS/A, and 122× for CT26. Murine germline alterations were subtracted by using normal DNA of BALB/c mice (for CT26 and TS/A) and FVB/N mice (for PDAC) previously sequenced at our institution. For calling mutations, we considered only positions present with a minimum depth of 5× (PDAC and TS/A) and 9× (CT26) and supported by at least 1% allelic frequency. Tumor mutational burden was evaluated as the number of variants per megabase considering those derived from coding regions. The prediction of neoantigens was performed using a bioinformatic pipeline we previously published (8, 60). Haplotypes for murine samples were set to H2-Kd and H2-Dd for the BALB/c background. Due to the lack of the *q* allele in the list of predicting tools, H2-Kk and H2-Ld were set for the FVB/N background. Only peptides with predicted strong binding affinity were considered.

Genomic Analysis on Patient Samples

Patient samples were identified from a pan-tumor MSI cohort treated with pembrolizumab monotherapy (ClinicalTrials.gov number NCT01876511). Response and progression were evaluated using RECIST 1.1 and the immune-related response criteria (61). To identify patients carrying tumors with *B2M* frameshift mutations, sequence analysis was performed as described previously (5). Briefly, formalin-fixed, paraffin-embedded blocks or frozen tissue sections were dissected to remove contaminating tissue (resulting in >20% neoplastic cells), and matched normal samples were provided for WES performed at Personal Genome Diagnostics, Inc. VariantDx custom software was used to identify putative somatic mutations. Candidate somatic mutations were further refined by identifying those occurring in protein-coding regions. LOH analysis was performed by FACETS (62), an allele-specific copy-number analysis tool that uses processed sequencing BAM files for joint segmentation of total and allele-specific read counts to detect copy-number aberrations in the genome. The cellular fraction feature in FACETS facilitates identification of clonal and subclonal copy-number events.

Immunofluorescence and Image Analysis

We used 38 pretreatment samples from the MSI pembrolizumab cohort for B2M staining (ab27588; Abcam) and MHC class I (HCA2, AM33034PU-N; Acris) immunofluorescence staining. Of the 38 samples, 20 specimens underwent an additional multiplex immunofluorescence panel with primary antibodies against CD8 (clone SP239, ab178089; Abcam), pan-cytokeratin (760-2595; Ventana), CD3 (clone SP162, ab135372; Abcam), and PD-L1 (clone SP263, 790-4905; Ventana). All staining procedures were automated on the BenchMark ULTRA automated slide stainer and scanned on the Zeiss AxioScan Z1. Slides were also stained with hematoxylin and eosin (Roche) and scanned using the iScanHT to annotate regions of interest. Image analysis was integrated within Roche Digital Pathology software to quantitate cell densities and characterize the tumor microenvironment.

RNA-seq and Inference of Infiltrating Immune Cells

Of the 38 pretreatment samples, 12 samples were annotated for the tumor region and underwent additional analyses with standard RNA-seq with rRNA depletion. Normalized gene expression data were then uploaded and applied to the CIBERSORT algorithm (http://cibersort.stanford.edu/) to infer the absolute abundance of multiple types of infiltrating immune cells. With a set of reference gene expression values ("signature matrix") for each immune cell type, CIBERSORT deconvolutes the tumor immune microenvironment from samples prepared from bulk tumors using support vector regression.

Statistical Analyses and Reproducibility

Statistical analyses were performed using Prism GraphPad software. During exome analysis, Fisher exact test was performed to calculate the significance of the frequency of each allele. For tissue culture experiments, statistical differences were calculated using paired Student *t* tests. To determine statistical significance for tumor growth, normality and log-normality tests were performed for each experiment. Because we did not find concordance among the Anderson–Darling, D'Agostino–Pearson, Shapiro–Wilk, and Kolmogorov–Smirnov tests, and considering the sample size, we exploited nonparametric tests (*P* values were adjusted with Mann–Whitney correction). We also used nonparametric tests for human data exploiting Mann–Whitney correction. The absence of *P* values in the figures reflects data that were not statistically significant ($P > 0.05$).

The number of replicates and sample size for *in vivo* experiments were limited according to requirements from the Italian Ministry of Health. Animal studies were performed in accordance with institutional guidelines and international law and policies. When therapy was applied, we performed randomization. In this case, tumor-free mice or mice with a tumor larger than 50% of the average were excluded from the experiment.

Data and Materials Availability

Raw sequencing data from WES of mouse cell lines present in the current study have been deposited in the European Nucleotide Archive with the following accession code: PRJEB41758.

Authors' Disclosures

G. Germano reports grants from NeoPhore; in addition, G. Germano has a patent (PCT/GB2017/051062) pending and licensed to NeoPhore/PhoreMost. B. Rousseau reports personal fees and non-financial support from Bayer, non-financial support from Servier, and personal fees from Roche and Gilead outside the submitted work. D. Stenech reports other support from NeoPhore during the conduct of the study. D.T. Le reports grants and personal fees from Merck during the conduct of the study, as well as personal fees from Bristol Myers Squibb and Janssen outside the submitted work; in addition, D.T. Le has a patent (WO2016077553A1) pending. J. Hays reports personal fees from Merck, Clovis, Tesaro, Ipsen, Deciphera, and AstraZeneca outside the submitted work. L.A. Diaz is a member of the board of directors of Personal Genome Diagnostics (PGDx) and Jounce Therapeutics. He is a compensated consultant to PGDx, 4Paws (PetDx), Innovatus CP, Se'er, Kinnate and Neophore. He is an uncompensated consultant for Merck but has received research support for clinical trials from Merck. L.A. Diaz is an inventor of multiple licensed patents related to technology for circulating tumor DNA analyses and mismatch repair deficiency for diagnosis and therapy from Johns Hopkins University. Some of these licenses and relationships are associated with equity or royalty payments directly to Johns Hopkins and L.A. Diaz. He holds equity in PGDx, Jounce Therapeutics, Thrive Earlier Detection, Se'er, Kinnate and Neophore. His spouse holds equity in Amgen. The terms of all these arrangements are being managed by Johns Hopkins and Memorial Sloan Kettering in accordance with their conflict of interest policies. A. Bardelli

Published OnlineFirst March 2, 2021; DOI: 10.1158/2159-8290.CD-20-0987

reports grants from AstraZeneca, NeoPhore, and AIRC. In addition, A. Bardelli has a patent (PCT-GB2017/051062) pending and licensed and is an inventor on patent applications related to this research. The transfer of certain materials to third parties is subject to terms contained within license and intellectual property agreements held between NeoPhore and the University of Turin. A. Bardelli is a cofounder and shareholder of NeoPhore Limited and is a member of the scientific advisory board of Horizon Discovery, NeoPhore, Biocartis, Cergentis, Guardant Health, Inivata, and Phoremost. No potential conflicts of interest were disclosed by the other authors.

One of the Editors-in-Chief is an author on this article. In keeping with the AACR's editorial policy, the peer review of this submission was managed by a member of *Cancer Discovery*'s Board of Scientific Editors, who rendered the final decision concerning acceptability.

Authors' Contributions

G. Germano: Conceptualization, data curation, formal analysis, validation, investigation, methodology, writing–original draft. **S. Lu:** Data curation, formal analysis. **G. Rospo:** Data curation, software, formal analysis. **S. Lamba:** Data curation, investigation, methodology. **B. Rousseau:** Data curation, formal analysis. **S. Fanelli:** Data curation, validation. **D. Stenech:** Data curation, validation. **D.T. Le:** Data curation, formal analysis. **J. Hays:** Data curation, formal analysis. **M.G. Totaro:** Data curation, methodology. **V. Amodio:** Data curation, formal analysis. **R. Chila:** Data curation. **A. Mondino:** Conceptualization, data curation, formal analysis, supervision, writing–original draft. **L.A. Diaz:** Conceptualization, data curation, formal analysis, supervision. **F. Di Nicolantonio:** Conceptualization, data curation, writing–original draft. **A. Bardelli:** Conceptualization, data curation, formal analysis, supervision, funding acquisition, validation, writing–original draft.

Acknowledgments

We thank members of the Molecular Oncology Laboratory at Candiolo Cancer Institute, FPO-IRCCS, and of the Department of Oncology, University of Torino, for critically reading the manuscript. We also thank Dr. A. Quintè, Dr. M.L. Sarnicola, Dr. M.C. Crosti, and Dr. D. Manganaro for help with flow cytometry experiments and Dr. Greta Brenna for statistical analysis. The research leading to these results has received funding from Fondazione AIRC under the 5 per Mille 2018–ID 21091 program (P.I. A. Bardelli, Group Leader F. Di Nicolantonio); AIRC under the IG 2018–ID 21923 project (P.I. A. Bardelli); European Community's Horizon 2020 (grant 635342-2 MoTriColor; A. Bardelli); an AIRC, CRUK, and FC AECC Accelerator Award (contract 22795; A. Bardelli); Fondazione Piemontese per la Ricerca sul Cancro-ONLUS 5 per mille 2014 and 2015 Ministero della Salute (A. Bardelli) and Strategy (F. Di Nicolantonio) projects; and Progetto NET-2011-02352137 Ministero della Salute (A. Bardelli). G. Germano was supported by Fondazione Umberto Veronesi and FPRC 5 per mille 2017 Ministero Salute PTCRC-Intra 2020 (REGENERATION-YIG 2020 project). L.A. Diaz, B. Rousseau, and D.T. Le are supported by a Stand Up To Cancer Colorectal Cancer Dream Team Translational Research grant (SU2C-AACR-DT22-17). Stand Up To Cancer is a division of the Entertainment Industry Foundation. The indicated Stand Up To Cancer grant is administered by the American Association for Cancer Research, the scientific partner of Stand Up To Cancer. B. Rousseau was supported by Nuovo-Soldati Foundation Funding and is now supported by a Swim Across America Foundation Fellowship.

The costs of publication of this article were defrayed in part by the payment of page charges. This article must therefore be hereby marked *advertisement* in accordance with 18 U.S.C. Section 1734 solely to indicate this fact.

Received July 9, 2020; revised January 9, 2021; accepted February 25, 2021; published first March 2, 2021.

REFERENCES

1. Ribas A, Wolchok JD. Cancer immunotherapy using checkpoint blockade. Science 2018;359:1350–5.
2. Wolchok JD, Kluger H, Callahan MK, Postow MA, Rizvi NA, Lesokhin AM, et al. Nivolumab plus ipilimumab in advanced melanoma. N Engl J Med 2013;369:122–33.
3. Migden MR, Rischin D, Schmults CD, Guminski A, Hauschild A, Lewis KD, et al. PD-1 blockade with cemiplimab in advanced cutaneous squamous-cell carcinoma. N Engl J Med 2018;379:341–51.
4. Santoni M, Montironi R, Battelli N. Immune checkpoint blockade in advanced renal-cell carcinoma. N Engl J Med 2018;379:91–2.
5. Le DT, Durham JN, Smith KN, Wang H, Bartlett BR, Aulakh LK, et al. Mismatch repair deficiency predicts response of solid tumors to PD-1 blockade. Science 2017;357:409–13.
6. Le DT, Uram JN, Wang H, Bartlett BR, Kemberling H, Eyring AD, et al. PD-1 blockade in tumors with mismatch-repair deficiency. N Engl J Med 2015;372:2509–20.
7. Overman MJ, Lonardi S, Wong KYM, Lenz HJ, Gelsomino F, Aglietta M, et al. Durable clinical benefit with nivolumab plus ipilimumab in DNA mismatch repair-deficient/microsatellite instability-high metastatic colorectal cancer. J Clin Oncol 2018;36:773–9.
8. Germano G, Lamba S, Rospo G, Barault L, Magri A, Maione F, et al. Inactivation of DNA repair triggers neoantigen generation and impairs tumour growth. Nature 2017;552:116–20.
9. Schrock AB, Ouyang C, Sandhu J, Sokol E, Jin D, Ross JS, et al. Tumor mutational burden is predictive of response to immune checkpoint inhibitors in MSI-high metastatic colorectal cancer. Ann Oncol 2019;30:1096–103.
10. Marcus L, Lemery SJ, Keegan P, Pazdur R. FDA approval summary: pembrolizumab for the treatment of microsatellite instability-high solid tumors. Clin Cancer Res 2019;25:3753–8.
11. Grasso CS, Giannakis M, Wells DK, Hamada T, Mu XJ, Quist M, et al. Genetic mechanisms of immune evasion in colorectal cancer. Cancer Discov 2018;8:730–49.
12. Gettinger S, Choi J, Hastings K, Truini A, Datar I, Sowell R, et al. Impaired HLA class I antigen processing and presentation as a mechanism of acquired resistance to immune checkpoint inhibitors in lung cancer. Cancer Discov 2017;7:1420–35.
13. Sade-Feldman M, Jiao YJ, Chen JH, Rooney MS, Barzily-Rokni M, Eliane JP, et al. Resistance to checkpoint blockade therapy through inactivation of antigen presentation. Nat Commun 2017;8:1136.
14. Zaretsky JM, Garcia-Diaz A, Shin DS, Escuin-Ordinas H, Hugo W, Hu-Lieskovan S, et al. Mutations associated with acquired resistance to PD-1 blockade in melanoma. N Engl J Med 2016;375:819–29.
15. Apcher S, Prado Martins R, Fåhraeus R. The source of MHC class I presented peptides and its implications. Curr Opin Immunol 2016;40:117–22.
16. Leone P, Shin EC, Perosa F, Vacca A, Dammacco F, Racanelli V. MHC class I antigen processing and presenting machinery: organization, function, and defects in tumor cells. J Natl Cancer Inst 2013;105:1172–87.
17. Halenius A, Gerke C, Hengel H. Classical and non-classical MHC I molecule manipulation by human cytomegalovirus: so many targets—but how many arrows in the quiver? Cell Mol Immunol 2015;12:139–53.
18. Schell TD, Mylin LM, Tevethia SS, Joyce S. The assembly of functional beta(2)-microglobulin-free MHC class I molecules that interact with peptides and CD8(+) T lymphocytes. Int Immunol 2002;14:775–82.

Published OnlineFirst March 2, 2021; DOI: 10.1158/2159-8290.CD-20-0987

19. Chapman DC, Williams DB. ER quality control in the biogenesis of MHC class I molecules. Semin Cell Dev Biol 2010;21:512–9.
20. Zügel U, Schoel B, Kaufmann SH. Beta 2-microglobulin independent presentation of exogenously added foreign peptide and endogenous self-epitope by MHC class I alpha-chain to a cross-reactive CD8+ CTL clone. J Immunol 1994;153:4070–80.
21. Hughes EA, Hammond C, Cresswell P. Misfolded major histocompatibility complex class I heavy chains are translocated into the cytoplasm and degraded by the proteasome. Proc Natl Acad Sci U S A 1997;94:1896–901.
22. Shukla SA, Rooney MS, Rajasagi M, Tiao G, Dixon PM, Lawrence MS, et al. Comprehensive analysis of cancer-associated somatic mutations in class I HLA genes. Nat Biotechnol 2015;33:1152–8.
23. Ijsselsteijn ME, Petitprez F, Lacroix L, Ruano D, van der Breggen R, Julie C, et al. Revisiting immune escape in colorectal cancer in the era of immunotherapy. Br J Cancer 2019;120:815–8.
24. Middha S, Yaeger R, Shia J, Stadler ZK, King S, Guercio S, et al. Majority of B2M-mutant and -deficient colorectal carcinomas achieve clinical benefit from immune checkpoint inhibitor therapy and are microsatellite instability-high. JCO Precis Oncol 2019;3: PO.18.00321.
25. Janikovits J, Muller M, Krzykalla J, Korner S, Echterdiek F, Lahrmann B, et al. High numbers of PDCD1 (PD-1)-positive T cells and B2M mutations in microsatellite-unstable colorectal cancer. OncoImmunology 2018;7:e1390640.
26. Restifo NP, Marincola FM, Kawakami Y, Taubenberger J, Yannelli JR, Rosenberg SA. Loss of functional beta 2-microglobulin in metastatic melanomas from five patients receiving immunotherapy. J Natl Cancer Inst 1996;88:100–8.
27. Cancer Genome Atlas Network. Comprehensive molecular characterization of human colon and rectal cancer. Nature 2012;487:330–7.
28. Propper DJ, Chao D, Braybrooke JP, Bahl P, Thavasu P, Balkwill F, et al. Low-dose IFN-gamma induces tumor MHC expression in metastatic malignant melanoma. Clin Cancer Res 2003;9:84–92.
29. Henriksen A, Dyhl-Polk A, Chen I, Nielsen D. Checkpoint inhibitors in pancreatic cancer. Cancer Treat Rev 2019;78:17–30.
30. Wein L, Luen SJ, Savas P, Salgado R, Loi S. Checkpoint blockade in the treatment of breast cancer: current status and future directions. Br J Cancer 2018;119:4–11.
31. Taylor MA, Hughes AM, Walton J, Coenen-Stass AML, Magiera L, Mooney L, et al. Longitudinal immune characterization of syngeneic tumor models to enable model selection for immune oncology drug discovery. J Immunother Cancer 2019;7:328.
32. Stockis J, Roychoudhuri R, Halim TYF. Regulation of regulatory T cells in cancer. Immunology 2019;157:219–31.
33. de Vries NL, van Unen V, Ijsselsteijn ME, Abdelaal T, van der Breggen R, Farina Sarasqueta A, et al. High-dimensional cytometric analysis of colorectal cancer reveals novel mediators of antitumour immunity. Gut 2020;69:691–703.
34. Hollern DP, Xu N, Thennavan A, Glodowski C, Garcia-Recio S, Mott KR, et al. B cells and T follicular helper cells mediate response to checkpoint inhibitors in high mutation burden mouse models of breast cancer. Cell 2019;179:1191–206.
35. Dhupkar P, Gordon N, Stewart J, Kleinerman ES. Anti–PD-1 therapy redirects macrophages from an M2 to an M1 phenotype inducing regression of OS lung metastases. Cancer Med 2018;7:2654–64.
36. Matsuzaki J, Tsuji T, Luescher IF, Shiku H, Mineno J, Okamoto S, et al. Direct tumor recognition by a human CD4(+) T-cell subset potently mediates tumor growth inhibition and orchestrates anti-tumor immune responses. Sci Rep 2015;5:14896.
37. Gao J, Aksoy BA, Dogrusoz U, Dresdner G, Gross B, Sumer SO, et al. Integrative analysis of complex cancer genomics and clinical profiles using the cBioPortal. Sci Signal 2013;6:pl1.
38. Cerami E, Gao J, Dogrusoz U, Gross BE, Sumer SO, Aksoy BA, et al. The cBio cancer genomics portal: an open platform for exploring multidimensional cancer genomics data. Cancer Discov 2012;2: 401–4.
39. Newman AM, Steen CB, Liu CL, Gentles AJ, Chaudhuri AA, Scherer F, et al. Determining cell type abundance and expression from bulk tissues with digital cytometry. Nat Biotechnol 2019; 37:773–82.
40. Newman AM, Liu CL, Green MR, Gentles AJ, Feng W, Xu Y, et al. Robust enumeration of cell subsets from tissue expression profiles. Nat Methods 2015;12:453–7.
41. Chen L. Co-inhibitory molecules of the B7-CD28 family in the control of T-cell immunity. Nat Rev Immunol 2004;4:336–47.
42. Diskin B, Adam S, Cassini MF, Sanchez G, Liria M, Aykut B, et al. PD-L1 engagement on T cells promotes self-tolerance and suppression of neighboring macrophages and effector T cells in cancer. Nat Immunol 2020;21:442–54.
43. Snyder A, Makarov V, Merghoub T, Yuan J, Zaretsky JM, Desrichard A, et al. Genetic basis for clinical response to CTLA-4 blockade in melanoma. N Engl J Med 2014;371:2189–99.
44. Torrejon DY, Abril-Rodriguez G, Champhekar AS, Tsoi J, Campbell KM, Kalbasi A, et al. Overcoming genetically based resistance mechanisms to PD-1 blockade. Cancer Discov 2020;10:1140–57.
45. Schietinger A, Philip M, Liu RB, Schreiber K, Schreiber H. Bystander killing of cancer requires the cooperation of CD4(+) and CD8(+) T cells during the effector phase. J Exp Med 2010;207: 2469–77.
46. Mumberg D, Monach PA, Wanderling S, Philip M, Toledano AY, Schreiber RD, et al. CD4(+) T cells eliminate MHC class II-negative cancer cells in vivo by indirect effects of IFN-gamma. Proc Natl Acad Sci U S A 1999;96:8633–8.
47. von Geldern M, Simm B, Braun M, Weiss EH, Schendel DJ, Falk CS. TCR-independent cytokine stimulation induces non-MHC-restricted T cell activity and is negatively regulated by HLA class I. Eur J Immunol 2006;36:2347–58.
48. Bogen B, Fauskanger M, Haabeth OA, Tveita A. CD4+ T cells indirectly kill tumor cells via induction of cytotoxic macrophages in mouse models. Cancer Immunol Immunother 2019;68:1865–73.
49. Salmon H, Idoyaga J, Rahman A, Leboeuf M, Remark R, Jordan S, et al. Expansion and activation of CD103(+) dendritic cell progenitors at the tumor site enhances tumor responses to therapeutic PD-L1 and BRAF inhibition. Immunity 2016;44:924–38.
50. Waldhauer I, Steinle A. NK cells and cancer immunosurveillance. Oncogene 2008;27:5932–43.
51. Freeman AJ, Vervoort SJ, Ramsbottom KM, Kelly MJ, Michie J, Pijpers L, et al. Natural killer cells suppress T cell-associated tumor immune evasion. Cell Rep 2019;28:2784–94.
52. Bern MD, Parikh BA, Yang L, Beckman DL, Poursine-Laurent J, Yokoyama WM. Inducible down-regulation of MHC class I results in natural killer cell tolerance. J Exp Med 2019;216:99–116.
53. Perez-Diez A, Joncker NT, Choi K, Chan WF, Anderson CC, Lantz O, et al. CD4 cells can be more efficient at tumor rejection than CD8 cells. Blood 2007;109:5346–54.
54. Nish S, Medzhitov R. Host defense pathways: role of redundancy and compensation in infectious disease phenotypes. Immunity 2011;34:629–36.
55. Nanni P, de Giovanni C, Lollini PL, Nicoletti G, Prodi G. TS/A: a new metastasizing cell line from a BALB/c spontaneous mammary adenocarcinoma. Clin Exp Metastasis 1983;1:373–80.
56. Bailey JM, Hendley AM, Lafaro KJ, Pruski MA, Jones NC, Alsina J, et al. p53 mutations cooperate with oncogenic Kras to promote adenocarcinoma from pancreatic ductal cells. Oncogene 2016;35: 4282–8.
57. Gilles ME, Maione F, Cossutta M, Carpentier G, Caruana L, Di Maria S, et al. Nucleolin targeting impairs the progression of pancreatic cancer and promotes the normalization of tumor vasculature. Cancer Res 2016;76:7181–93.
58. Woerner SM, Tosti E, Yuan YP, Kloor M, Bork P, Edelmann W, et al. Detection of coding microsatellite frameshift mutations in DNA mismatch repair-deficient mouse intestinal tumors. Mol Carcinog 2015;54:1376–86.

Published OnlineFirst March 2, 2021; DOI: 10.1158/2159-8290.CD-20-0987

59. Corti G, Bartolini A, Crisafulli G, Novara L, Rospo G, Montone M, et al. A genomic analysis workflow for colorectal cancer precision oncology. Clin Colorectal Cancer 2019;18:91–101.
60. Germano G, Amirouchene-Angelozzi N, Rospo G, Bardelli A. The clinical impact of the genomic landscape of mismatch repair-deficient cancers. Cancer Discov 2018;8:1518–28.
61. Wolchok JD, Hoos A, O'Day S, Weber JS, Hamid O, Lebbé C, et al. Guidelines for the evaluation of immune therapy activity in solid tumors: immune-related response criteria. Clin Cancer Res 2009;15:7412–20.
62. Shen R, Seshan VE. FACETS: allele-specific copy number and clonal heterogeneity analysis tool for high-throughput DNA sequencing. Nucleic Acids Res 2016;44:e131.

AACR American Association for Cancer Research

CANCER DISCOVERY

CD4 T Cell–Dependent Rejection of Beta-2 Microglobulin Null Mismatch Repair–Deficient Tumors

Giovanni Germano, Steve Lu, Giuseppe Rospo, et al.

Cancer Discov 2021;11:1844-1859. Published OnlineFirst March 2, 2021.